Neuron
Article

Parvalbumin-Positive Basket Cells Differentiate among Hippocampal Pyramidal Cells

Sang-Hun Lee,[1,4,*] Ivan Marchionni,[1,2,4] Marianne Bezaire,[1] Csaba Varga,[1] Nathan Danielson,[3] Matthew Lovett-Barron,[3,5] Attila Losonczy,[3] and Ivan Soltesz[1,2]
[1]Department of Anatomy and Neurobiology
[2]Center for Autism Research and Treatment
University of California, Irvine, CA 92697, USA
[3]Department of Neuroscience, Columbia University, New York, NY 10032, USA
[4]Co-first author
[5]Present address: Department of Bioengineering, Stanford University, Stanford, CA 94305, USA
*Correspondence: sanghun.lee@uci.edu
http://dx.doi.org/10.1016/j.neuron.2014.03.034

SUMMARY

CA1 pyramidal cells (PCs) are not homogeneous but rather can be grouped by molecular, morphological, and functional properties. However, less is known about synaptic sources differentiating PCs. Using paired recordings in vitro, two-photon Ca^{2+} imaging in vivo, and computational modeling, we found that parvalbumin-expressing basket cells (PVBCs) evoked greater inhibition in CA1 PCs located in the deep compared to superficial layer of stratum pyramidale. In turn, analysis of reciprocal connectivity revealed more frequent excitatory inputs to PVBCs by superficial PCs, demonstrating bias in target selection by both the excitatory and inhibitory local connections in CA1. Additionally, PVBCs further segregated among deep PCs, preferentially innervating the amygdala-projecting PCs but receiving preferential excitation from the prefrontal cortex-projecting PCs, thus revealing distinct perisomatic inhibitory interactions between separate output channels. These results demonstrate the presence of heterogeneous PVBC-PC microcircuits, potentially contributing to the sparse and distributed structure of hippocampal network activity.

INTRODUCTION

The mammalian hippocampus plays a critical role in learning and memory processes, by transforming input from associative neocortical regions and sending output primarily through long-distance projecting pyramidal cells (PCs) in the CA1 region. These outputs target a number of brain areas, including the medial prefrontal cortex (mPFC), medial entorhinal cortex (MEC), and amygdala (AMG) (Cenquizca and Swanson, 2007), potentially coordinating the interactions among brain areas during mnemonic functions (Maren and Quirk, 2004; Fanselow and Poulos, 2005). Heterogeneity across the CA1 PC population is recognized along the radial axis (superficial to deep), marked by differential expression of the neurochemical markers (e.g., calbindin and zinc; Figure 1A), and in long-range projection patterns (Baimbridge and Miller, 1982; Slomianka et al., 2011). Whereas the CA1 region as a whole is known to be the general output of the hippocampus proper, how the heterogeneous PCs integrate into the CA1 circuit remains unknown.

In particular, it is unclear what the nature of the relationship is between heterogeneity of PCs (Bannister and Larkman, 1995; Mizuseki et al., 2011; Deguchi et al., 2011; Graves et al., 2012) and the well-known diversity of local GABAergic hippocampal interneurons (Soltesz, 2005). Specifically, given the heterogeneous structural and functional properties of PCs in CA1, the question arises if all PCs are regulated by essentially identical local GABAergic circuits or whether hippocampal interneurons nonuniformly target specific subpopulations of CA1 PCs. The issue of heterogeneity in target selection by cortical interneurons is controversial. Some reports suggest that local GABAergic microcircuits in various cortical areas can be selective for different postsynaptic populations (Fariñas and DeFelipe, 1991; Yoshimura and Callaway, 2005; Bodor et al., 2005; Otsuka and Kawaguchi, 2009; Varga et al., 2010; Gittis et al., 2010; Viviani et al., 2011; Lee et al., 2014; for a review, see Krook-Magnuson et al., 2012). In contrast, others reported a lack of preference in target selection for a variety of neocortical interneurons, including parvalbumin- (Packer and Yuste, 2011) and somatostatin-positive interneurons (Fino and Yuste, 2011). The lack of clear evidence for or against the differential regulation of distinct subpopulations of CA1 PCs by local inhibitory circuits limits our understanding of hippocampal network operations.

Among local microcircuits of the hippocampus, the interactions between PCs and perisomatic-targeting, fast-spiking, parvalbumin-expressing basket cells (PVBCs) (Figure 1B) have been extensively studied and inexorably linked to hippocampal rhythmogenesis (for a review, see Buzsáki and Wang, 2012). The importance of these interneurons is also highlighted by the fact that PVBCs have been implicated, both within and outside the hippocampus, in local circuit operations, learning and memory, sensory processing, and critical period plasticity; aberrant PVBC activities may also be mechanistically linked to

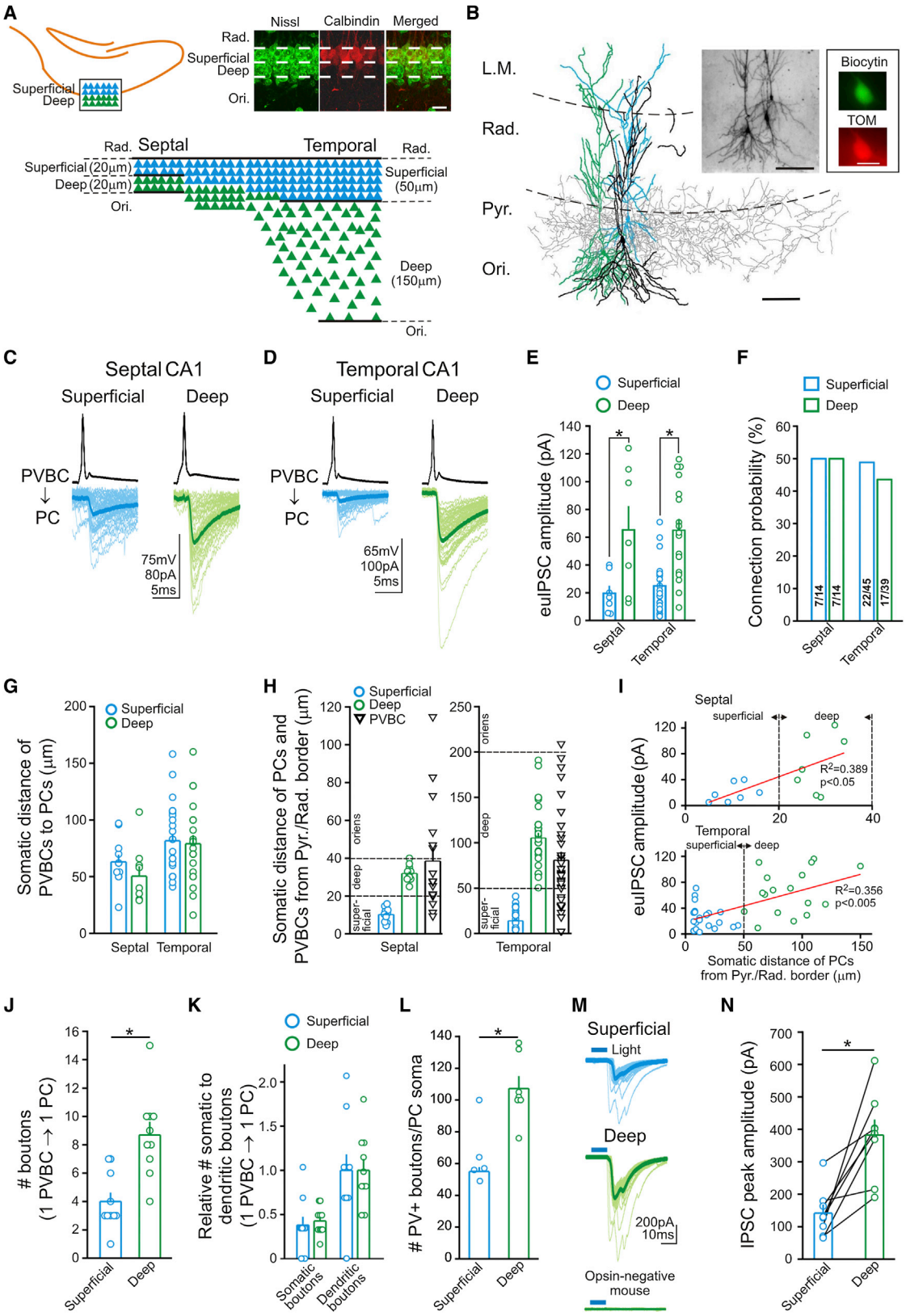

(legend on next page)

neurological and psychiatric disorders including epilepsy, autism, and schizophrenia (Pouille and Scanziani, 2004; Lewis et al., 2005; Ogiwara et al., 2007; Gibson et al., 2009; Armstrong and Soltesz, 2012; Lee et al., 2012; Verret et al., 2012; Trouche et al., 2013; Kuhlman et al., 2013). Therefore, we focused on these key GABAergic cells to test the hypothesis that interneurons can be selective with respect to the heterogeneity of PC populations to nonuniformly regulate distinct hippocampal output channels. In addition, we also examined the other, nonoverlapping basket cell population, the cholecystokinin-expressing basket cells (CCKBCs) (Armstrong and Soltesz, 2012), since the latter cells have been shown to be highly selective in establishing perisomatic synapses with specific postsynaptic target cell populations in MEC (Varga et al., 2010).

In order to test the relationship between PVBC and CCKBC target selection and PC heterogeneity, we used in vitro paired intracellular recordings, in vivo two-photon functional imaging in awake mice, and computational modeling. The data showed that PVBCs evoked several times greater postsynaptic currents in CA1 PCs located in the deep compared to the superficial sublayer of stratum pyramidale. In sharp contrast, CCKBCs did not show any selectivity with regard to these PC subpopulations. Analysis of reciprocal connectivity revealed greater excitation of PVBCs by superficial PCs, suggesting the existence of highly preferential excitatory-inhibitory interactions between the PC subpopulations and the PVBCs. A computational network model incorporating our experimental findings indicated that the newly uncovered, biased PC-PVBC connectivity can give rise to a preferential feedforward inhibition from the superficial to deep pyramidal cell sublayer. Furthermore, we also found that PVBCs preferentially innervated PCs projecting to the amygdala but received preferential excitatory innervation from PCs that projected to the prefrontal cortex, thus revealing directionally biased local circuit interactions between separate output channels. These results demonstrate that hippocampal local inhibitory-excitatory circuits involving PVBCs form nonuniform connectivity motifs with various heterogeneous PC populations that may contribute to the sparse and distributed structure of hippocampal network activity.

RESULTS

PVBCs Preferentially Innervate Subpopulations of CA1 PCs

In vivo, the more than 40-mm-long axonal arborization of a single PVBC in the CA1 has over 10,000 putative presynaptic boutons, covering an area of about 1 mm^2 where an estimated 10,000 PCs reside (Halasy et al., 1996; Bezaire and Soltesz, 2013). However, in spite of the similarity of the number of boutons and potential target cells, single PVBCs innervate only about 10% of the PCs within their axonal cloud, forming multiple, basket-like synaptic contacts on the somata and proximal dendrites of the innervated PCs (Bezaire and Soltesz, 2013). If individual PVBCs do not form synapses with all potential PCs within their reach, how do they choose their poststynaptic targets? Is the target selection a random process where a given PVBC selects some PCs by chance, or do these interneurons preferentially innervate a specific subset of PCs that share some common characteristics? In order to differentiate between these two possibilities, we set out to investigate whether the innervation patterns of PVBCs are related to the heterogeneity of CA1 PCs. Namely, we first tested the hypothesis that PVBCs preferentially innervated PCs based on the location of the PCs within the deep (closer to the stratum oriens) versus superficial (closer to the stratum radiatum) sublayers of the stratum pyramidale (Figures 1, 2, 3, 4, and 5). Next, we also examined whether preferential innervation of PCs by PVBCs existed based on the differential long-distance projection targets of the postsynaptic PCs (Figure 6). The deep/superficial PC sublayers were defined as follows (see Figure 1A; in the septal [dorsal] CA1: superficial sublayer: 0–20 μm; deep sublayer: 20–40 μm; in the temporal [ventral] CA1: superficial sublayer: 0–50 μm; deep sublayer: 50–200 μm; for detailed explanations and rationale, see Supplemental Experimental Procedures available online).

Figure 1. Nonuniform Targeting of CA1 PCs by PVBCs

(A) Top left: schematic drawing illustrates the deep and superficial subdivisions of the CA1 somatic layer. Bottom: differences in the cellular compactness and width of the deep and superficial sublayers along septotemporal (dorsoventral) axis of the hippocampus (see also Section 4 in Supplemental Experimental Procedures and Slomianka et al., 2011). Top right: calbindin expression in the superficial sublayer in the septal CA1. Scale bar, 20 μm. Rad., stratum radiatum; Ori., oriens.

(B) The reconstruction of a superficial (blue) and a deep PC (green) innervated by a common presynaptic PVBC (soma and dendrites, black; axons, gray). L.M., stratum lacunosum-moleculare; Pyr., stratum pyramidale. Scale bar, 100 μm. Insets: light microscope image of the PVBC, sPC, and dPC (top left); scale bar, 100 μm; tdTomato (TOM, top right) expression in the recorded PVBC; scale bar, 10 μm.

(C and D) Representative traces from paired recordings in the septal (C) and temporal (D) CA1, showing IPSCs (averages: thick lines) in an sPC (blue) and dPC (green) evoked by APs in the presynaptic PVBCs.

(E) Summary data of the "effective unitary" IPSCs (euIPSCs).

(F) Connection probability from PVBCs to PCs. Numbers in bars indicate connected/tested pairs.

(G) Summary of somatic distances between the PVBC-sPC or PVBC-dPC pairs in the septal (left) and temporal (right) CA1 in (C)–(F).

(H) Distances from the Pyr/Rad border of the paired recorded PCs and PVBCs in the septal (left) and temporal (right) CA1.

(I) Plots of euIPSC amplitude against distance of PCs from Pyr/Rad border; red lines, linear fits to data.

(J) Number of putative axon terminals of single PVBCs on single sPCs (n = 10) and dPCs (n = 10).

(K) Relative number of somatic to proximal dendritic boutons of single PVBCs on single sPCs (n = 10) and dPCs (n = 10); data normalized by the average number of dendritic boutons in each group.

(L) Summary data of the number of putative synaptic PV^+ boutons around the somata of biocytin-filled dPCs and sPCs.

(M) Example traces from d/sPCs in response to blue light (10 ms) in slices from PV-ChR2-expressing mice; note lack of light-evoked IPSCs in opsin-negative mice.

(N) Summary data of the optogenetic experiments. Means and SEM are plotted. *$p < 0.05$ in all figures. See also Figure S1.

In order to determine the presence or absence of sublayer-specific patterns of postsynaptic PC innervation by PVBCs, we performed paired recordings from presynaptic PVBCs and postsynaptic deep (dPCs) or superficial PCs (sPCs) in acute hippocampal slices from mice expressing *tdTomato* in PV^+ neurons. Because PV expression alone does not unequivocally define PVBCs (since there are other PV^+ cells in CA1, including the dendritically projecting bistratified cells, and the axon initial segment-targeting axoaxonic or chandelier cells), every PVBC in this study was identified based on post hoc visualization of the axonal arbor (Figure 1B). Note that, in agreement with previous morphological studies (Bannister and Larkman, 1995), there were some morphological differences between the dPCs and sPCs, with the dPCs having larger basal dendritic trees and somata (Figures S1A–S1D). There were no differences between dPCs and sPCs in terms of their firing frequency as a function of intracellularly injected current (Figure S1E) and in input resistance (Figure S1F). However, sPCs showed more depolarized resting membrane potentials (Figure S1G) and, as reported before (Jarsky et al., 2008), larger sag potentials in response to large hyperpolarizing current pulses (Figure S1H). Thus, sPCs and dPCs are morphologically and physiologically distinct groups.

The paired recordings revealed that the synaptic currents generated by PVBCs in sPCs and dPCs were far from uniform. Rather, action potentials in PVBCs evoked inhibitory postsynaptic currents (IPSCs) in dPCs that were almost three times larger than the IPSCs in sPCs, both in the septal and temporal hippocampus (Figures 1C–1E; IPSC amplitudes including both successful events and failures, referred to as "effective" unitary IPSCs [euIPCs]: septal: dPC: 65.2 ± 17.2 pA, n = 7; sPC: 19.6 ± 5.4 pA, n = 7; $p < 0.05$; temporal: dPC: 65.0 ± 8.3 pA, n = 17; sPC: 24.9 ± 3.9 pA, n = 22; $p < 0.005$). Note that the difference in IPSC amplitudes was significant also when only the successful events were considered (referred to as "unitary" IPSC amplitudes [uIPSCs]: dPC: 68.4 ± 6.9 pA, n = 24; sPC: 32.4 ± 3.5 pA, n = 29; data pooled from septal and temporal CA1, $p < 0.005$). Furthermore, the robust difference in IPSC amplitudes was present without a difference in connection probability (ratio of connected and unconnected pairs during the paired recordings) (Figure 1F; septal: sPCs: 50%; dPCs: 50%; temporal: sPCs: 48.9%; dPCs: 43.6%). The larger events in the dPCs were not due to a preferential spatial arrangement of the pre- with respect to the postsynaptic cells, since the somatic distances of the PVBC-sPC pairs (76.2 ± 4.7 μm; n = 38) and the PVBC-dPC pairs (70.4 ± 6.3 μm; n = 30) were not different ($p > 0.5$; Figure 1G; the somata of the recorded sPCs and dPCs were distributed throughout the respective sublayers [Figure 1H]; the somata of the recorded PVBCs were located in both the superficial and the deep PC sublayers and in the stratum oriens [Figure 1H]). In addition, the larger euIPSCs in dPCs compared to sPCs were also observed when the postsynaptic cells shared a common presynaptic PVBC (n = 8 sequential paired recordings; dPC: 63.8 ± 15.9 pA; sPC: 22.1 ± 5.5 pA; $p < 0.001$). These data demonstrated that PVBCs showed selectivity in innervation patterns with respect to their CA1 PC targets.

There was, however, variability of the recorded euIPSC amplitudes within both sPC and dPC groups and overlap in recorded amplitudes between groups (see Figure 1E). While there was a correlation between distance of the postsynaptic PCs from the stratum radiatum and the euIPSC amplitude (Figure 1I; R^2 = 0.389, $p < 0.05$, septal CA1; R^2 = 0.356, $p < 0.005$, temporal CA1), this was driven by the overall difference between sPCs and dPCs, as no correlation remained when examining either group individually (R^2 = 0.027, p = 0.22, sPC; R^2 = 0.045, p = 0.20, dPC; data from temporal CA1, where the number of data points was high enough for R^2 statistics even after splitting data into two groups). Rather, it appeared that there were large- and small-amplitude euIPSCs in both groups, with more "large"-amplitude euIPSCs recorded from dPCs. Therefore, we performed a K-means test for two-clusters, which indicated a "small"-amplitude euIPSC cluster with a mean of 22.5 pA, and a "large"-amplitude cluster with a mean of 82.1 pA. The recorded average euIPSCs were significantly more likely to be "large" amplitude when recorded from a dPC (3 of 22 average euIPSCs recorded from sPCs were "large" amplitude versus 10 of 17 from dPCs, $p < 0.01$, Pearson's chi-square test). This suggests that, although PVBCs did evoke significantly larger events in dPCs than in sPCs on average, the location of the PC somata was not a perfect predictor of euIPSC amplitude. Therefore, in a later part of the study, we also examined euIPSC amplitudes in PCs within the same sublayer but with different projection targets (see below and Figure 6).

Morphological analysis of the pairs of recorded cells revealed that PVBCs formed significantly more perisomatic axon terminals on dPCs compared to sPCs (Figures 1J and S1I; dPC: 8.7 ± 0.9, n = 10; sPC: 4.0 ± 0.6, n = 10; $p < 0.005$), presenting structural evidence for an unequal innervation of PCs by PVBCs in the CA1 (note that the recovery rates of somata and proximal/distal dendrites after paired recordings were similar between sPCs and dPCs, indicating that the unequal PVBC innervation of the PCs was not due to a slicing artifact; Figure S1J). The presence of more boutons from single PVBCs on dPCs versus sPCs was consistent with the larger euIPSCs in dPCs. In support of the latter mechanism involving more presynaptic terminals and thus more GABA release sites on dPCs, the PVBC-to-dPC unitary inputs were accompanied by smaller coefficient of variation (dPC: 0.61 ± 0.06, n = 17; sPC: 1.00 ± 0.06, n = 22; $p < 0.001$) and larger probability of success in GABA release (dPC: 0.92 ± 0.03, n = 17; sPC: 0.66 ± 0.04, n = 22; $p < 0.001$), without differences in short-term plasticity properties (amplitude of the second uIPSC as a percentage of the first in response to two closely spaced presynaptic action potentials; dPC: 71.6% ± 7.6%, n = 17; sPC: 88.9% ± 9.9%, n = 22; $p > 0.3$). Furthermore, additional morphological analysis showed that the ratio of the number of somatic versus proximal dendritic PVBC boutons was similar between PVBC-sPC and PVBC-dPC pairs (Figure 1K; $p > 0.38$), indicating that the differences in euIPSC amplitudes could not be explained by a higher preference for the somata of dPCs by the PVBC inputs.

Next, we set out to test the above physiological and structural findings by independent means. Namely, we predicted that the total number of PVBC boutons on individual dPCs should be approximately double that of the sPCs, because the electrophysiology experiments showed that the connection probability was similar between individual PVBCs and dPCs or sPCs

(suggesting similar convergence), but single PVBCs formed about twice as many boutons on dPCs compared to sPCs. Therefore, we performed an immunocytochemical analysis of the overall PV boutons on biocytin-filled individual sPCs and dPCs. In agreement with our prediction, the results showed that the number of PV^+ boutons around the somata of single dPCs were approximately 2-fold higher than in the case of sPCs (dPC: 107.3 ± 7.8, n = 7; sPC: 55.0 ± 2.8, n = 5; $p < 0.005$) (Figures 1L and S1K). Taken together, these data indicated that a similar number of PVBCs converged onto single dPCs and sPCs, but individual PVBCs provided more boutons onto dPCs compared to sPCs.

Finally, we set out to determine whether activation of a population of heterogeneous PV^+ cells (and not just individual PVBCs specifically) could evoke preferentially larger inhibitory events in dPCs. Optogenetic experiments were performed in hippocampal slices from PV-ChR2 mice that expressed the excitatory opsin channelrhodopsin (ChR2) selectively in PV^+ cells. Activation of PV^+ interneurons with blue light while dual patch-clamp recording from a dPC and an sPC resulted in significantly larger optogentically evoked IPSCs in dPCs compared to sPCs (dPC: 382.3 ± 47.8 pA, n = 8; sPC: 141.6 ± 26.3 pA, n = 8; $p < 0.005$; the light-evoked events were abolished by the $GABA_A$ receptor antagonist gabazine, 20 μM, n = 3; the light-evoked IPSCs were absent in opsin-negative animals, n = 3) (Figures 1M and 1N). These optogenetic results showed that PV^+ cell activation in general was able to evoke preferentially larger inhibitory synaptic events in dPCs.

Running Evokes Preferential Activation of PVBC Axon Terminals around the Somata of dPCs

In order to investigate the relevance of the above-described differential synaptic arrangement between PVBCs and PCs to behaving animals, we used two-photon Ca^{2+} imaging to record activity from PV^+ axon terminals in the CA1 PC layer of head-fixed mice running on a treadmill (Figure 2A; Kaifosh et al., 2013). We selectively expressed the genetically encoded Ca^{2+} indicator GCaMP5 (Akerboom et al., 2012) in PV^+ interneurons of the CA1 and focused our imaging plane to the superficial and deep PC sublayers to record Ca^{2+}-evoked fluorescence from axonal boutons surrounding the somata of unlabeled PCs. In agreement with the previously described running-associated elevation in the firing of identified PVBCs (Varga et al., 2012), we observed robust increases in PV^+ axonal fluorescence in each field of view (FOV) during running (gray bars under traces in Figure 2B) compared to the nonrunning state. Importantly, the running-associated increases in full-field axonal fluorescence were significantly larger in the deep compared to the superficial sublayer (Figures 2B and 2C; deep: $\Delta F/F$ = 43.4% ± 3.7%; superficial: 30.3% ± 2.4%; n = 10 superficial-deep FOV pairs in 5 mice; $p < 0.05$), in agreement with the electrophysiological and structural data described in the previous section.

The observed larger increases in PV^+ axonal fluorescence in the deep compared to the superficial sublayer could have been caused by stronger activation of PV^+ boutons in the deep sublayer or the presence of more PV^+ boutons in the deep sublayer or both. In order to differentiate between these possibilities, we examined the running-associated increases in fluorescence in regions of interest (ROIs) around PV^+ boutons. The fluorescence of PV^+ ROIs increased in both layers during running (Figure 2D), but there was no difference in the enhancement in PV^+ bouton ROI fluorescence between the sublayers (Figure 2E; deep: $\Delta F/F$ = 60.4% ± 6.2%, n = 5; superficial: 59.3% ± 7.2%, n = 5; $p > 0.5$). The latter imaging data were in overall agreement with the in vitro electrophysiology results that indicated no differences in short-term plasticity properties at PVBC-dPC versus PVBC-sPC synapses (see above). In addition, in order to ascertain that our imaging techniques were able to reveal the stronger PV^+ innervation of the deep compared to the superficial sublayer, we performed PV^+ bouton counts in anesthetized mice using two-photon imaging in vivo and found significantly higher numbers of PV^+ boutons in the deep compared to the superficial sublayer (Figure 2F).

The in vivo imaging results indicated that the preferential innervation of the dPCs by the PVBCs observed in the in vitro paired recording experiments and morphological studies described above was not due to a slice artifact. However, a potential concern in interpreting the in vivo imaging data is that, in addition to PVBCs, the PV^+ axoaxonic (chandelier) cells also provide innervation of PCs within the pyramidale layer. Therefore, especially since the postsynaptic domains targeted by the axoaxonic cells (the axon initial segments) are situated on the side of the PC somata that is closer to the stratum oriens, it is possible that the observed difference in PV^+ axonal fluorescence between the sublayers was due to a preferential innervation of the deep layer by the axoaxonic cells. In order to investigate the latter potential confound, we performed triple immunocytochemical experiments using antibodies against PV, AnkG (a marker for axon initial segments), and VGAT (for presynaptic GABAergic terminals) and confocal microscopy to quantify PV^+ axon initial segment-targeting and somatic/proximal dendritic boutons (Figure S2A; PV^+ boutons within 0.5 μm from $AnkG^+$ profiles were considered initial segment-targeting boutons; all other PV^+ boutons within the stratum pyramidale were classified as somatic/proximal dendritic boutons). The results showed that 12.7% (229 out of 1,803) of the PV^+ boutons in the deep sublayer and 4.2% (49 out of 1,161) of the PV^+ boutons in the superficial sublayer were axon initial segment-targeting boutons. Therefore, 87.3% (deep) and 95.8% (superficial) were somatic/proximal dendritic-targeting PV^+ boutons (i.e., originating from PVBCs) (Figure S2B). We then used the latter data to correct for the contribution of the axon initial segment-targeting PV^+ boutons to the imaging results. These calculations showed significantly larger increases in running-associated elevations in fluorescence in the deep compared to the superficial sublayer even from the PVBC-associated PV^+ boutons alone (corrected $\Delta F/F$, deep: 37.9% ± 3.3%; superficial: 29.0% ± 2.2%; $p < 0.05$).

As a final control for the in vivo imaging experiments and for the in vitro electrophysiological and structural results, we examined the sublayer-specific distributions of boutons belonging to single PVBCs that were filled with biocytin in either in vitro (using whole-cell recordings) or in vivo (using juxtacellular recordings) experiments in the septal hippocampus. These bouton counts were performed in the approximate planes in the stratum pyramidale from which the two-photon in vivo imaging results were also obtained (superficial: 0 μm to 10 μm; deep: 20 μm to 30 μm). The

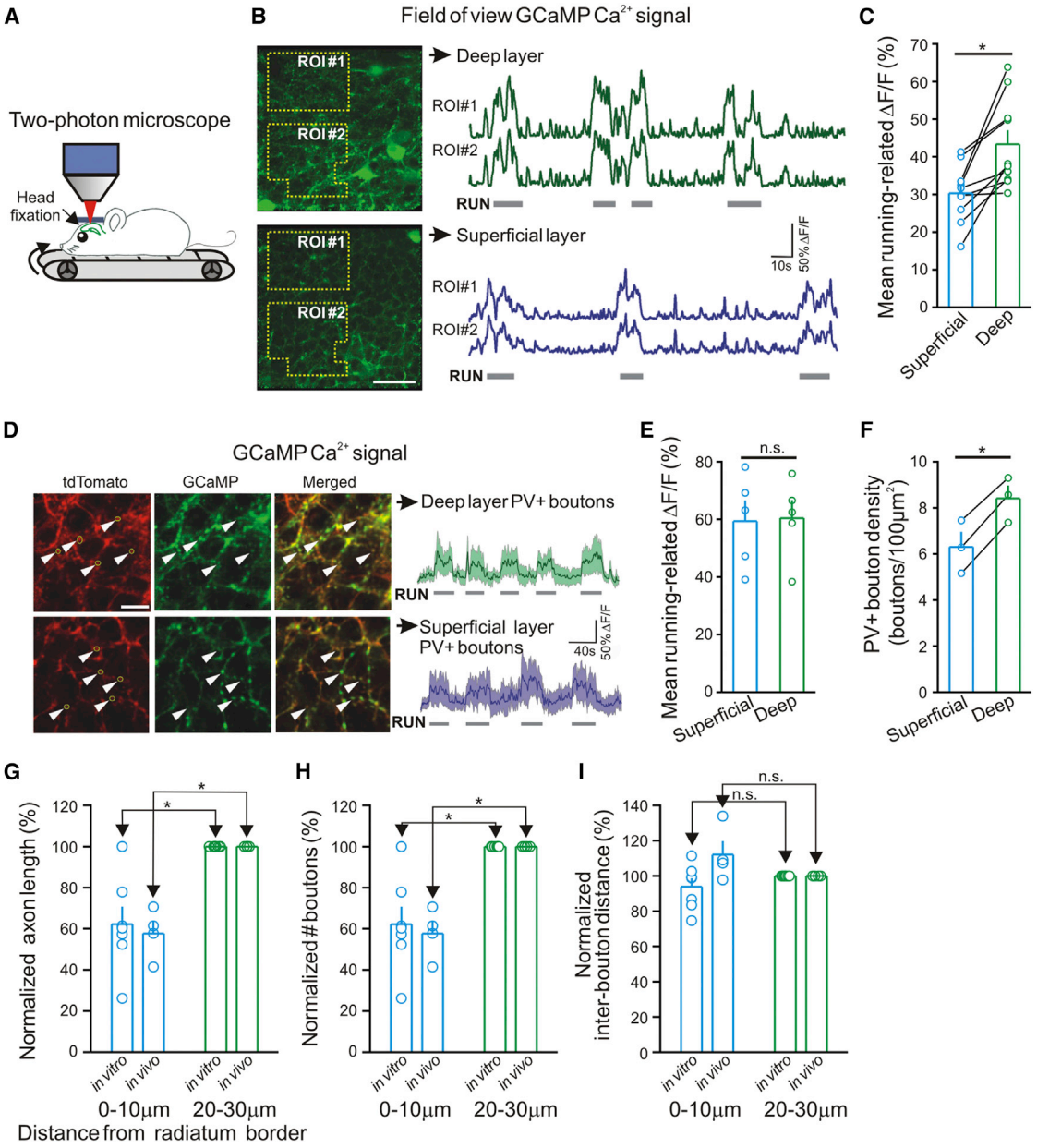

Figure 2. Running-Evoked Differential Rises in PV-Driven GCaMP Ca^{2+} Signal around dPCs and sPCs

(A) Schematic of in vivo two-photon imaging experiments.

(B) Left: example time-averaged fluorescence images (2,000 frames) from the superficial and deep sublayers of the CA1 stratum pyramidale in the dorsal (septal) CA1. Relative change in GCaMP Ca^{2+} fluorescence (ΔF/F) was first calculated over two to four polygonal regions of interest (ROIs) for superficial and deep-imaging planes and then averaged within FOVs. Wide-field ROIs were selected to avoid somatic or dendritic profiles of PV^+ interneurons in both imaging planes; scale bar, 40 μm. Right: example ΔF/F traces from the two ROIs in superficial and deep sublayers. Horizontal bars indicate periods of running.

(C) Summary of mean relative GCaMP Ca^{2+} fluorescence change during running activity in FOVs.

(D) Left: example time-averaged fluorescence images from superficial and deep sublayers taken at high magnification (red, tdTomato; green, GCaMP). Bouton ROIs (yellow circles show five examples; arrowheads point to the areas of the circles) were selected based on the stationary tdTomato signal. Scale bar, 10 μm. Right: representative fluorescence traces (all boutons in FOV with a response between 0% and 200% ΔF/F) of GCaMP Ca^{2+} signals in superficial and deep sublayers. Horizontal bars indicate periods of running activity.

(E) Summary of mean running-evoked GCaMP Ca^{2+} signal in perisomatic PV^+ boutons compared across the two sublayers.

(F) Summary of bouton density per 100 μm^2 in the two sublayers.

(G, H, and I) Summary of morphological measurements of the length (G), number of boutons (H), and interbouton distance (I) of axons originating from individual PVBCs filled in vitro and in vivo in the septal CA1. Means and SEM are plotted. n.s., not significant (in this and subsequent figures). See also Figure S2.

analysis showed significantly longer axons (Figure 2G) and more boutons (Figure 2H) belonging to single PVBCs in the deep compared to the superficial sublayer, regardless of whether the PVBCs were filled in vitro (n = 7) or in vivo (n = 4). Interestingly, the interbouton distance was not different (Figure 2I). Taken together, these PVBC axonal arbor data further substantiated our in vivo imaging and in vitro electrophysiology and morphology results.

In summary, the results described so far presented comprehensive evidence from a variety of in vitro and in vivo functional and structural approaches for the preferential innervation by PVBCs of the CA1 PCs located in the deep sublayer of the stratum pyramidale. Although the relative degree of the difference between the preferential PVBC innervation of the deep compared to the superficial sublayer showed a wide range with the various in vitro and in vivo methods, there was unanimity in the results in that all electrophysiological, optogenetic, morphological, and imaging approaches indicated significant differences in the PVBC innervation patterns as a function of the sublayers.

CA1 sPCs Are More Likely to Provide Excitatory Inputs to PVBCs

PVBCs do not inhibit PCs in isolation but rather are embedded in excitatory-inhibitory loops with PCs within CA1 (Pouille and Scanziani, 2004). Therefore, we next investigated the cell-type specificity of the local excitatory inputs to PVBCs by examining PVBC-PC pairs in the reverse order. We found that the connection probability between sPCs to PVBCs was three times higher compared to dPCs to PVBCs (Figures 3A and 3C; dPC: 16%, 8/50 pairs connected; sPC: 48.2%, 27/56; $p < 0.001$), with no difference in the euEPSC amplitudes (Figure 3B; dPC: 33.3 ± 5.1 pA, n = 8; sPC: 46.7 ± 10.7 pA, n = 27; $p > 0.1$). In addition, there was no difference in the probability of success in glutamate release from dPCs (0.74 ± 0.06, n = 8) versus sPCs (0.70 ± 0.05, n = 27; $p < 0.05$), and the short-term plasticity properties were also similar between the two groups (dPC: 89.1% ± 16.7%, n = 8; sPC: 82.3% ± 9.8%, n = 18; $p > 0.5$).

These data demonstrated that sPCs provided more excitatory connections to PVBCs compared to dPCs, without a difference in presynaptic properties. Therefore, it was the PC group that received smaller GABAergic inputs from the PVBCs (the sPCs) that provided more excitation to these interneurons. These data suggested the presence of a local circuit motif that may preferentially route PVBC-mediated perisomatic inhibition from sPCs to dPCs (the degree of bias in the sPC-PVBC-dPC synaptic connections is illustrated in Figure 3D, where the length of the arrows was made to be proportional to the mean eul/EPSC amplitude times the connection probability; note that meaningful comparison can be made between similar-colored arrows only, representing the excitatory or inhibitory connections).

Next, we investigated these network motifs further. Results from the neocortex showed that the synaptic connections between pairs of excitatory cells and fast-spiking interneurons depended on whether the connection was reciprocal or present only in one direction (Yoshimura and Callaway, 2005). Analysis of our paired recording data revealed that, at the level of individual cell pairs, PVBCs formed unitary connections with similar probability and strength with sPCs regardless of whether the sPCs provided excitatory input to the PVBC (Figure 3E). A similar scenario was observed for dPCs (Figure 3F). Therefore, these data indicated differences in small network motifs between neocortical and hippocampal circuits.

PVBCs Nonuniformly Inhibit the Action Potential Discharges of PCs

The data presented so far showed a preferential innervation of the dPCs by PVBCs compared to sPCs. Does the preferential PVBC innervation translate to more efficacious inhibition of dPC action potentials (APs)? In order to answer this question, we employed paired current-clamp recordings from presynaptic PVBCs and postsynaptic sPCs or dPCs in slices. Intracellular depolarizing current pulses were injected into the presynaptic PVBCs to cause them to fire APs with an intraburst frequency of 40 Hz (gamma frequency) and an interburst frequency of 7 Hz (theta frequency), in order to mimic the discharge patterns of PVBCs during running-associated theta-gamma oscillations (Varga et al., 2012). In addition, the postsynaptic PCs were also made to fire in a manner that resembled the physiological situation, by using depolarizing current injections to arrive at firing rates similar to the PC discharge frequency in behaving rats (Lapray et al., 2012) (sPC: 2.2 ± 0.1 Hz, n = 8; dPC: 2.1 ± 0.2 Hz, n = 7; $p > 0.5$; note also that the pipettes used to record from the postsynaptic PCs contained 4 mM chloride, close to the normal intracellular [Cl^-]). As illustrated in Figure 4A, the gamma-burst firing PVBCs were able to inhibit the APs in dPCs to a significantly greater degree than in sPCs (Figures 4B; change in dPCs firing during theta-nested gamma-frequency discharges of PVBCs: 2.1 ± 0.2 Hz to 0.6 ± 0.2 Hz, n = 7; in sPC: from 2.2 ± 0.1 Hz to 1.6 ± 0.3 Hz, n = 8; $p < 0.05$). These results demonstrate that CA1 PVBCs were able to confer larger perisomatic inhibition to preferentially decrease spiking in dPCs.

Computational Simulations Indicate Preferential Feedforward Inhibition from the Superficial to Deep PC Sublayer

Next, we turned to computational modeling in order to gain a better understanding of whether the observed differences in connectivity of sPCs and dPCs with PVBCs may be significant in a network context. Our computational model was biologically constrained by our experimental observations (including the intrinsic and inhibitory and excitatory synaptic properties described above; Figure S3; see also Supplemental Experimental Procedures) and consisted of 1,000 sPCs, 1,000 dPCs, and 36 PVBCs, following the ratio of CA1 PCs to PVBCs previously determined (Bezaire and Soltesz, 2013). We then excited all cells in the network with equivalent, random, Poisson-distributed excitatory inputs. Under control conditions, the individual cells had physiologically realistic average firing rates of about 2.4 Hz for the dPC and sPC (Figure 4C, left-hand column, Control). We then selectively increased the excitation to either the sPCs (middle column) or to the dPCs (right-hand column) by adding 5%, 10%, 15%, 20%, 30%, or 40% extra CA3 inputs to all cells of the given PC type.

We noted two main effects of the increased excitation. First, increasing excitation selectively to sPCs in the model caused a

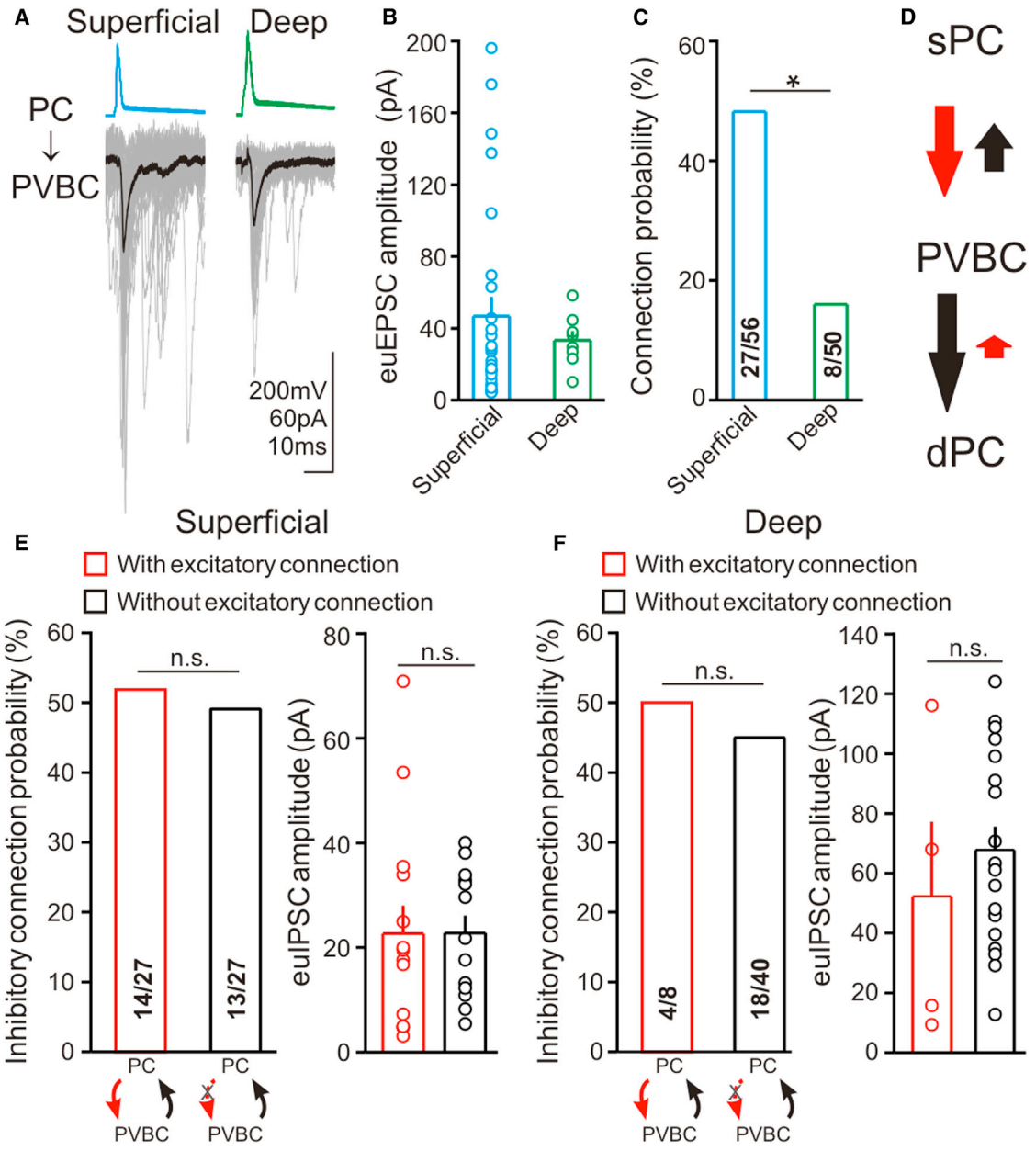

Figure 3. Preferential Excitatory Innervation of PVBCs by sPCs and Uni- versus Bidirectionally Connected Two-Cell Network Motifs

(A) Example traces of APs in PCs and EPSCs evoked in postsynaptic PVBCs (averages: thick lines).

(B) "Effective unitary" EPSC amplitudes (euEPSCs; both successful events and failures) evoked by sPCs (blue) versus dPCs (green).

(C) PC to PVBC connection probability from paired recordings.

(D) Schematic representation of the data in Figures 1 and 3.

(E and F) Two-cell (excitation/inhibition) small network motifs from paired recordings. PVBCs showed similar unitary inhibitory connection probabilities and euIPSC amplitudes with individual sPCs independent of whether or not excitatory input existed from the sPC to the PVBC (E). Similar results were found for PVBC to dPC connections as well (F). Numbers in bars: connected/tested pairs. Means and SEM are plotted.

larger decrease in dPC firing than the decrease in sPC firing that occurred after increasing excitation selectively to dPCs (Figure 4D; $p < 0.001$), and the sPCs in the network (subject to less PVBC inhibition) were more sensitive to increasing levels of excitation than the dPCs (Figures 4E; note that the I-F curves, reflecting intrinsic excitability, were similar in the two groups, both in the model and experimental PCs; Figures S1E and S3D). Second, increasing the firing rate of the dPC and sPC by similar amounts had differing effects on the PVBC firing rates (Figure 4F). The latter result was true even when similar PC firing rates were concerned (as opposed to similar increases in excitation). For example, adding an additional 5% of excitatory inputs

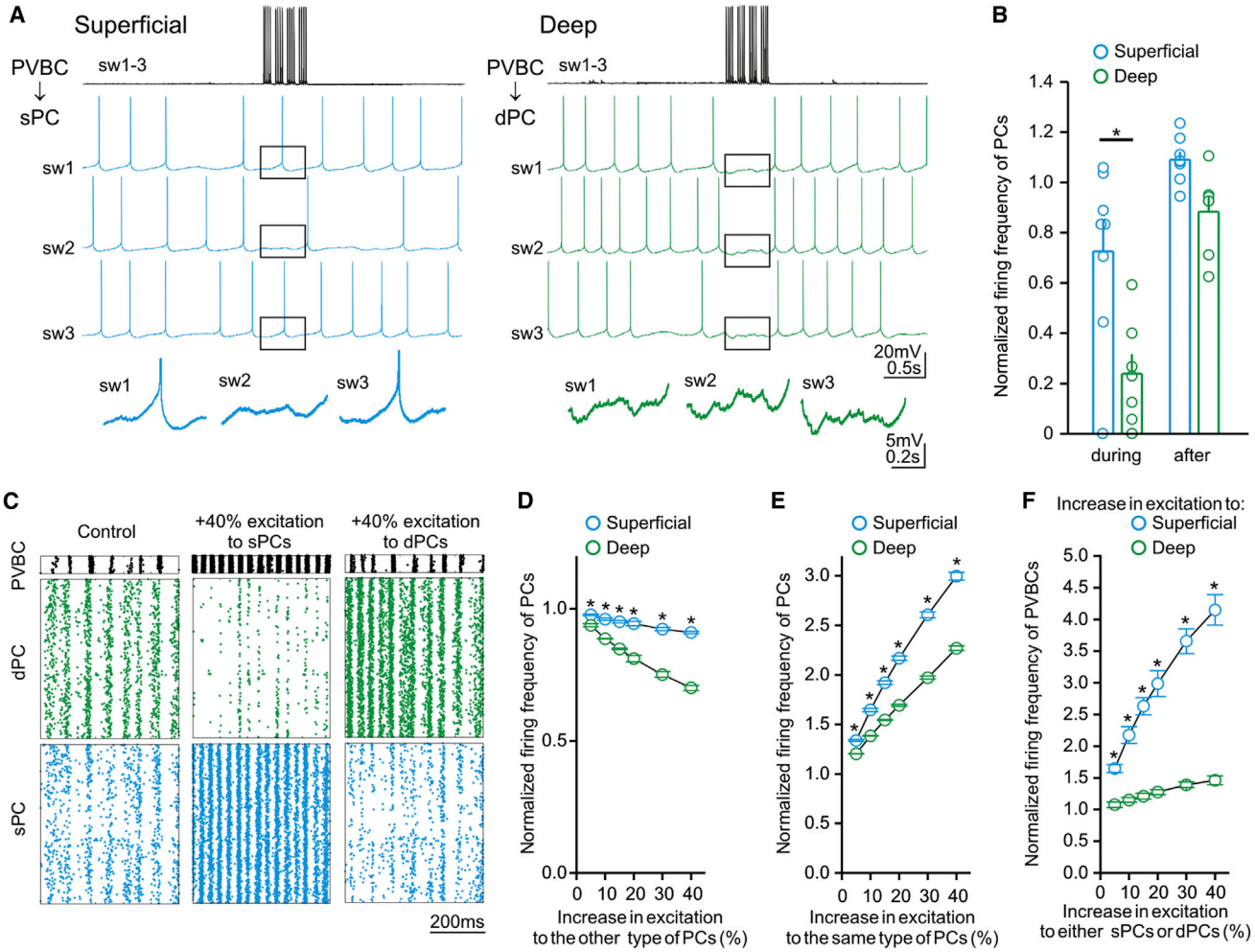

Figure 4. Preferential Inhibition of APs in dPCs by PVBCs

(A) Examples traces (sw, sweeps) from paired recorded PVBCs and s/dPCs.

(B) Summary of normalized firing frequency during and after train of APs in PVBCs.

(C) Raster plots illustrating spiking in the biologically constrained computer network model (see Results and Experimental Procedures for details).

(D, E, and F) Summary of three statistically independent simulations showing the differential changes in firing frequency of s/dPCs and PVCBs in response to selective increases in excitation. The effects on sPC and dPC firing rates are shown as a result of increased excitation to the other type of pyramidal cell (D) or the same type of pyramidal cell (E). The effect on PVBC firing rate is shown for increased excitation from either pyramidal cell type (F). Means and SEM are plotted. See also Figure S3 and Table S1.

to the sPCs increased the sPC firing rate by 34% (Figure 4E), which was similar to the effect of adding an additional 10% of excitatory inputs to the dPCs that increased the dPC firing rate by 38%. However, these similar increases in PC firing rates differently affected the PVBC firing rate. While a 34% increase in sPC firing rate resulted in a 65% increase in PVBC firing, a 38% increase in dPC firing rate only resulted in a 15% increase in PVBC firing (Figure 4F). Therefore, our network model that incorporated our experimental data exhibited directionally biased feedforward inhibition between sPCs and dPCs.

Cholecystokinin-Expressing Basket Cells Do Not Preferentially Innervate CA1 sPCs versus dPCs

The second, nonoverlapping class of basket cells is the PV^{-}, CCKBCs, which possess distinct electrophysiological and functional properties (Armstrong and Soltesz, 2012). In layer II of the medial entorhinal cortex, CCKBCs have been shown to selectively choose their postsynaptic targets (Varga et al., 2010). Do CCKBCs in the CA1 also preferentially innervate dPCs compared to sPCs? To answer this question, we performed paired recordings from presynaptic CCKBCs and postsynaptic dPCs or sPCs (Figure 5A). These paired recordings revealed that the IPSCs generated by the CCKBCs were similar between sPCs and dPCs (Figures 5B and 5C; eIPSCs amplitude; dPC: 42.2 ± 8.5 pA, n = 20; sPC: 42.9 ± 8.8 pA, n = 21; $p > 0.5$; data from the temporal hippocampus). In addition, there was also no difference in connection probability (Figure 5D; dPC: 44%; sPC: 40%; $p > 0.62$). The somatic distance of the recorded cells in the CCKBC-sPC (150.8 ± 8.3 μm, n = 25) and CCKBC-dPC (157.8 ± 8.2 μm, n = 22) pairs was

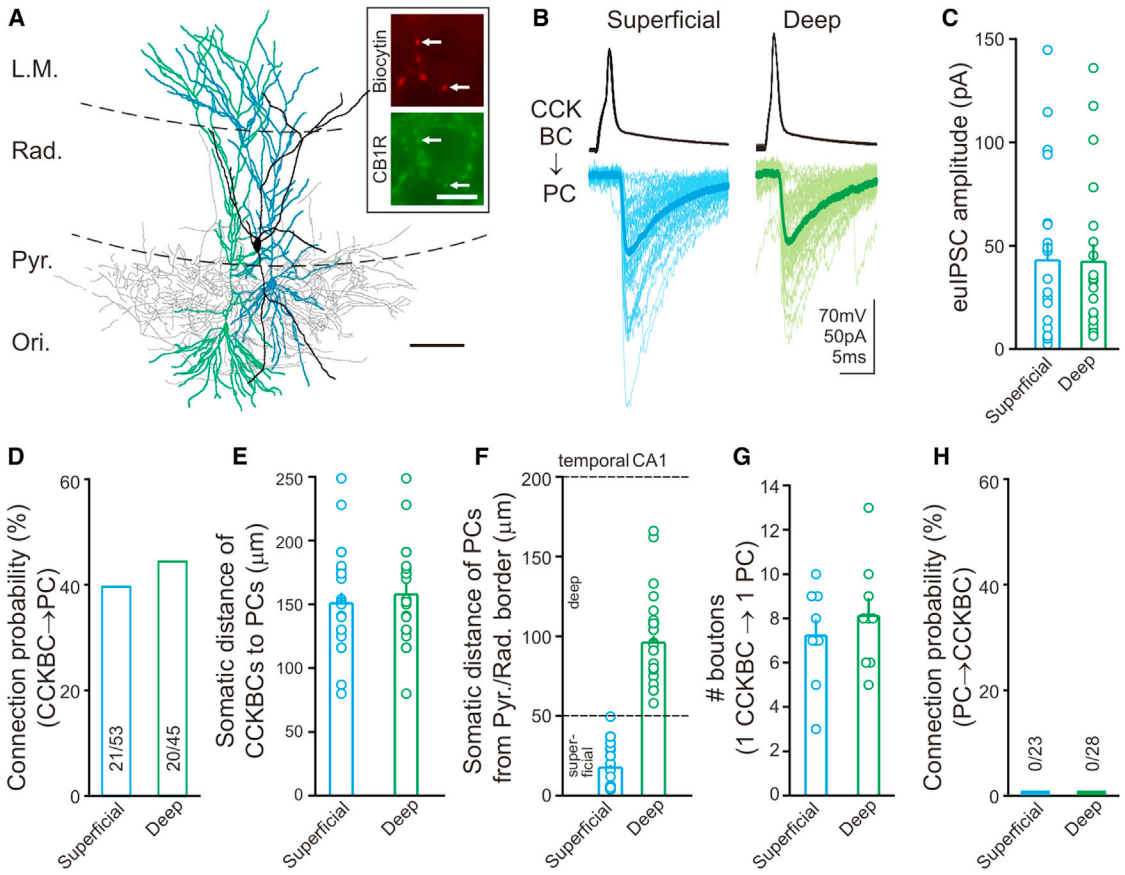

Figure 5. Lack of Preferential Innervation between s/dPCs and CCKBCs

(A) Reconstruction of an sPC (blue), a dPC (green), and a CCKBC (soma and dendrites, black; axons, gray); scale bar, 100 μm. Inset: CB1R expression in the CCKBC boutons; scale bar, 10 μm.

(B) Representative traces from a presynaptic CCKBC and dPC (green) and sPC (blue) in the presence of CB1R antagonist AM251 (10 μM) to block the tonic inhibition of GABA release from CCKBCs (Lee et al., 2010).

(C–F) Summary data of euIPSC amplitudes (C), connection probability between CCKBCs to PCs (D), somatic distances between CCKBC-sPC and CCKBC-dPC pairs in the temporal CA1 (E), and somatic locations of the paired recorded s/dPCs with respect to the Pyr/Rad border (F).

(G) Number of putative synaptic terminals of single CCKBCs onto single sPCs and dPCs (n = 9 for both).

(H) Excitatory connection probability from PCs to CCKBCs. Means and SEM are plotted. See also Figure S4.

similar ($p > 0.5$; Figure 5E; for location of the PCs, see Figure 5F). In agreement with the lack of difference in euIPSC amplitudes, morphological analysis of the pairs showed that CCKBCs formed a similar number of perisomatic boutons on dPCs compared to sPCs (Figure 5G; $p > 0.5$). Furthermore, we found no difference in the number of $CB1R^+$ boutons around the somata of sPCs and dPCs (Figures S4A and S4B; $p > 0.5$), suggesting that the convergence of CCKBCs onto single sPCs and dPCs was similar. Of interest, we did not find excitatory connections from dPCs or sPCs to CCKBCs (Figure 5H; deep: 0/28 connected; superficial: 0/23 connected; to our knowledge, there has also been no direct demonstration of excitatory connections between CA1 PCs and morphologically identified CCKBCs in the literature). Together, these results demonstrate that CCKBCs, in stark contrast to PVBCs, do not differentiate between superficial and deep CA1 PCs, which is an unexpected finding in light of their selectivity in MEC (Varga et al., 2010).

Heterogeneous PVBC Microcircuits as a Function of Long-Distance Targets of CA1 PCs

Our results above add to a growing body of evidence suggesting that the CA1 PC population is organized into distinct subgroups (Slomianka et al., 2011). This heterogeneity, however, is not limited to radial position, as CA1 PCs within a sublayer may project to distinct targets (Slomianka et al., 2011; Graves et al., 2012). As mentioned above, we had noted the presence of a certain degree of heterogeneity in the amplitude of PVBC-derived euIPSCs among the dPCs and sPCs (Figures 1E and 1I). Therefore, we next sought to investigate whether PVBCs further segregate PCs according to their efferent connectivity.

First, we needed to identify a specific, restricted volume of CA1 where PCs with differential long-distance projection targets could be found in similar septotemporal and dorsoventral positions to allow paired recordings to be performed from presynaptic PVBCs and the differentially projecting postsynaptic PCs

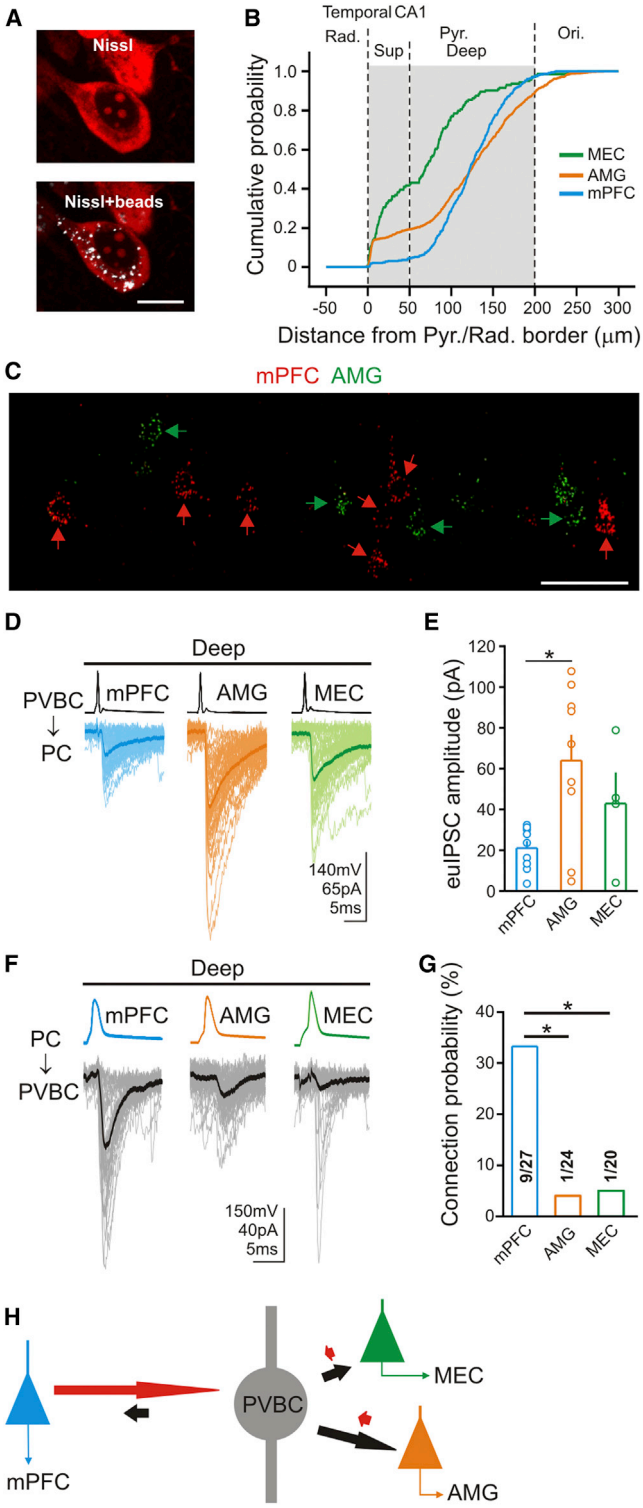

Figure 6. Heterogeneous Microcircuits between PVBCs and dPCs with Different Long-Distance Axonal Projection Targets

(A) Example of a retrogradely labeled PC in Nissl-stained material used to generate data (B); scale bar, 10 μm.

(B) Cumulative probability distributions of soma location of dPCs projecting to MEC (green), AMG (orange), or mPFC (blue) from the temporal hippocampus.

without confounds related to potential differences in cellular or functional properties in distinct parts of the hippocampus (e.g., Jung et al., 1994). A series of experiments using retrograde tracers (Figure 6A) indicated that PCs that projected to the mPFC, MEC, or AMG (Figure S5A) could be found in a restricted area of the temporal hippocampus (septotemporal position, A-P: 3.1 to 3.7 mm from Bregma) at the level of the rhinal fissure (±480 μm from the rhinal fissure in the dorsoventral direction). The MEC-projecting PCs ($_{MEC}$PCs) were abundant in both the deep and the superficial sublayers, while the mPFC-projecting PCs ($_{mPFC}$PCs) were almost exclusively located in the deep sublayer, and the AMG-projecting PCs ($_{AMG}$PCs) were also primarily in the deep sublayer (Figure 6B). Since all three types of long-distance projecting PC could be found in the deep sublayer, we focused on that sublayer in the subsequent experiments in order to separate the issue of the sublayer-specific innervation of PCs by PVBCs (Figures 1, 2, 3, 4, and 5) from the question of whether PVBCs show selectivity in terms of the long-distance projection targets of PCs.

Next, we examined the question of whether PCs projecting to distinct areas form largely parallel pathways or whether the same PC typically projects to several areas. In order to answer this question, we focused on $_{mPFC}$PCs and $_{AMG}$PCs, as they appeared to be more abundant compared to the $_{MEC}$PCs in the deep sublayer of the temporal hippocampus after our injections of retrograde tracers (Figure S5B; note that these relative abundance values should not be considered to be necessarily an accurate reflection of the total number of PCs projecting to the three areas, as the relative numbers of retrogradely labeled dPCs would be influenced by the injected tracer volume relative to the tissue volume and other factors, and the relative numbers would also be expected to be different in distinct septotemporal parts of the hippocampus). When different-colored retrograde tracers were injected into the mPFC and AMG, the majority of the labeled CA1 dPCs were labeled only with one of the two tracers (Figures 6C and S5C; note the intermingling of the labeled cells in the deep sublayer in Figure 6C; $_{mPFC}$PCs also labeled from AMG: 17%, 54 colabeled cells out of 314 cells; $_{AMG}$PCs also labeled from mPFC: 14%, 54/385 colabeled cells; n = 3 animals), indicating that the $_{mPFC}$PCs and $_{AMG}$PCs form a largely segregated, parallel projection pathway from the CA1. These results were in agreement with previous reports indicating that differentially projecting CA1 PCs form mostly parallel pathways, probably processing distinct modalities of information (Cenquizca and Swanson, 2007; Graves et al., 2012).

(C) Confocal image of retrogradely labeled dPCs after ipsilateral double injections of fluorescent microspheres into mPFC (red beads) and AMG (green beads). Green arrows, $_{AMG}$PCs; red arrows, $_{mPFC}$PCs; scale bars, 50 μm.

(D) Representative traces from presynaptic PVBCs (top) and postsynaptic $_{mPFC}$dPCs, $_{AMG}$dPCs, or $_{MEC}$dPCs.

(E) Summary of eIPSC amplitudes.

(F) Representative traces from differentially projecting presynaptic dPCs and postsynaptic PVBCs.

(G) Summary of connection probabilities.

(H) Schematic representation of data from (D)–(G); length of red and black arrows is proportional to mean eIPSC amplitudes times connection probability. Means and SEM are plotted. See also Figure S5.

For a narrated animation of Figure 6, see the figure online at http://dx.doi.org/10.1016/j.neuron.2014.03.034#mmc4.

The paired recordings in slices from animals preinjected with the retrograde tracers revealed that PVBCs evoked significantly larger euIPSCs in postsynaptic $_{AMG}$PCs compared to $_{mPFC}$PCs (Figures 6D and 6E; AMG: 64.0 ± 12.6 pA, n = 9; mPFC: 21.0 ± 3.5 pA, n = 9; $p < 0.05$; the uIPSC amplitudes were also larger in $_{AMG}$PCs compared to $_{mPFC}$PCs [Figure S5D]; there was no difference in probability of GABA release [Figure S5E] or in connection probability: PVBC-$_{mPFC}$PCs: 32.1%, 9/28 pairs; PVBC-$_{AMG}$PCs: 36%, 9/24 pairs). These results, demonstrating a 3-fold larger average euIPSC in $_{AMG}$PCs compared to $_{mPFC}$PCs, showed that the selectivity of PVBCs existed not only in terms of the superficial versus deep sublayers, but also with regards to the differential long-distance targets of PCs within a sublayer. The difference in euIPSCs evoked by PVBCs in $_{mPFC}$PCs versus $_{AMG}$PCs was not due to differences in the relative positions of the recorded cells (Figures S5F–S5H) or PC morphology (Figures S5I and S5J), and the recovery rates of the PC somata and proximal/distal dendrites after the paired recordings were also similar, indicating that the results were unlikely to be due to a differential slicing effect (Figure S5K). In addition, morphological analysis of the recorded cell pairs showed that PVBCs formed significantly more perisomatic axon terminals on $_{AMG}$PCs compared to $_{mPFC}$PCs (AMG: 6.0 ± 0.4, n = 4; mPFC: 3.0 ± 0.4, n = 4; $p < 0.005$), providing structural evidence for the preferential innervation of PVBCs of differentially projecting CA1 PCs.

Finally, we also examined the excitatory connectivity between the $_{mPFC}$PCs or $_{AMG}$PCs or $_{MEC}$PCs and the PVBCs during our paired recording experiments. The data showed that $_{mPFC}$PCs were significantly more likely than $_{AMG}$PCs or $_{MEC}$PCs to display excitatory connections with PVBCs (Figures 6F and 6G; mPFC: 33.3%; AMG: 4.2%; MEC: 5%; $p < 0.025$; note that because of the extremely low excitatory connection probability between the $_{AMG/MEC}$PCs and PVBCs, differences in euEPSC amplitudes could not be determined: $_{mPFC}$PCs: 19.5 ± 5.5 pA, n = 9; $_{AMG}$PC: 10.9 pA, n = 1; $_{MEC}$PC: 6.1 pA, n = 1). Therefore, these data showed that $_{mPFC}$PCs contacted PVBCs with almost eight times higher probability compared to $_{AMG}$PCs, demonstrating the presence of selectivity in excitatory innervation patterns between differentially projecting PCs and PVBCs, even within the same sublayer. Furthermore, similar to what was described above for the sPCs-PVBC-dPC connections (Figure 3D), it was again those PCs that received significantly smaller inhibitory input from PVBCs (in this case, the $_{mPFC}$PCs) that were more likely to provide excitatory innervation of these interneurons. Thus, similar to the directionality we observed between the PC sublayers, these data suggested the existence of a biased microcircuit arrangement within the deep sublayer that appears to be well suited to preferentially regulate distinct hippocampal output channels (Figure 6H).

DISCUSSION

Fine-Scale Organization of Hippocampal Perisomatic Fast Inhibition

What is the fine-scale organization of fast GABAergic inhibition in cortical networks? Is it a form of "blanket inhibition" characterized by an unspecific, homogenous matrix covering PCs, as indicated by recent results from neocortical PV^+ interneurons (Packer and Yuste, 2011) and SOM+ cells (Fino and Yuste, 2011)? Or is the nature of the GABAergic microcircuit organization such that individual interneuron subtypes are selective with respect to principal cell subpopulations (Krook-Magnuson et al., 2012)? The answer to these questions is important not only for understanding the organization of cortical interneuronal microcircuits in general, but also for PVBCs in particular, since the latter cells play key roles in normal hippocampal operations and various disorders.

Our results provide comprehensive evidence for the existence of specialized inhibitory microcircuits targeting functionally distinct subpopulations of hippocampal CA1 PCs. CA1 PVBCs, both in the septal and temporal hippocampus, evoked several times larger IPSCs in dPCs, formed higher number of boutons on dPC somata, and evoked stronger inhibition of APs in dPCs compared to sPCs. The two-photon in vivo imaging results were in general agreement with the paired recording in vitro data, as well as the in vivo and in vitro structural results, showing higher running-associated increases in PV^+ bouton fluorescence in the deep PC layer, even after correcting for the PV^+ axoaxonic synapses. Furthermore, PVBCs proved to be selective not only with respect to sublayers, but also in terms of the long-distance projection targets of PCs within a single sublayer, as PVBCs preferentially innervated $_{AMG}$dPCs.

Taken together, these data demonstrate that PVBCs do not provide uniform ("blanket") inhibition to CA1 PCs. Therefore, PVBCs not only release GABA at specific postsynaptic compartments (somata and proximal dendrites) at specific times (Varga et al., 2012), but they do so in a selective manner that confers preferential inhibition to PCs with distinct sublayer positions and long-distance targets. Our findings are consistent with recent in vivo data from freely moving animals that revealed differences in the firing patterns of CA1 dPCs and sPCs during theta oscillations (Mizuseki et al., 2011). Moreover, our data demonstrating the existence of heterogeneous PVBC innervation of differentially projecting dPCs are also in general agreement with the heterogeneity observed among the dPC population in the Mizuseki et al. (2011) study, where a large proportion of dPCs, but not all, shifted their preferred phase of firing during REM-associated theta. Our results from the hippocampus are also consistent with data from the neocortex indicating selectivity of PV^+ cells (Lee et al., 2014) and striatum (Gittis et al., 2010), supporting the emerging view that interneurons have the potential to selectively regulate specific information-processing streams represented by subpopulations of principal cells with distinct long-range projection targets (for a review, see Krook-Magnuson et al., 2012).

Local PVBC-PC Network Motifs

In addition to the striking selectivity of the PVBC-derived hippocampal perisomatic inhibition, the data in this paper also revealed an unexpected, inverse relationship between the inhibitory and excitatory connections. Namely, while sPCs received less inhibition from PVBCs, the excitatory connections from the

sPCs on the PVBCs were significantly more frequent compared to the dPC-to-PVBC synapses. The latter finding was closely mirrored by the results from the differentially projecting dPC subpopulations, where, again, it was the PC subpopulation that received the weaker PVBC inhibition (the $_{mPFC}$dPCs) that provided more frequent excitation to the PVBCs. Although the significance of these inversely correlated, selective inhibitory and excitatory circuit arrangements is not yet fully understood, our strictly data-driven computational network model that incorporated the experimental results on intrinsic and synaptic properties exhibited robust, directionally biased feedforward inhibition in the CA1 microcircuit following increases in incoming excitation. It is also interesting to note that the probability of connection and the strength of the PVBC-evoked IPSCs did not depend on whether the PC connected back to the PVBC (this was true for both the sPCs and dPCs; Figures 3E and 3F). These results were different than what was found in the neocortex (Yoshimura and Callaway, 2005), indicating that the fine structure of the excitatory-inhibitory small network motifs may differ between brain regions.

Limitations of the Study

A major strength of the current study is that every paired recorded interneuron was rigorously identified post hoc as a PVBC based on its axonal arborization, in order to differentiate these cells from other PV$^+$ cells. Similarly, every putative CCK cell was also post hoc identified specifically as a CCKBC, to differentiate it from the also CCK$^+$ Schaffer collateral-associated cells that innervate PC dendrites (Lee et al., 2010). Such meticulous identification of the two types of basket cell was important for the purposes of the current study, since there is increasing evidence that the heterogeneous members of the PV- or CCK-expressing families play distinct roles in the network (Szabadics et al., 2006; Lee et al., 2010). Therefore, while the current study provided proof of concept for the existence of interneuronal specificity for target selection of PC subpopulations within the hippocampus, it will be important to carry out future investigations to address the question of which other interneuronal subtypes within the PV and CCK families and beyond may offer similar target selectivity, either in terms of sublayers and/or long-distance projection targets. Indeed, it is interesting to note that the highest selectivity displayed by interneurons in terms of synaptically targeted subpopulations reported to date is the case of the CCKBCs in MEC (Varga et al., 2010), where CCKBCs virtually completely avoided (reelin-expressing) layer II cells that projected to the ipsilateral dentate gyrus. In spite of the stunning selectivity of CCKBCs in MEC, however, CCKBCs in the CA1 were not selective for sPC/dPC subpopulations, highlighting our incomplete understanding of the principles underlying the organization of preferential GABAergic synaptic networks targeting specific PC groups.

In addition, although the various electrophysiological, morphological, and imaging approaches all indicated significant differences in the PVBC innervation patterns as a function of the sublayers, there appeared to be a difference in the relative magnitude of the preferential PVBC innervation of the deep versus superficial sublayer as assessed with in vivo calcium imaging (~40% larger in the deep sublayer) and paired recordings (~200% larger IPSCs in the deep sublayer). However, it is important to note that the in vivo calcium imaging reports changes in calcium signals in PV$^+$ boutons in the imaging planes in the superficial and deep sublayers, but PV$^+$ boutons make synaptic contacts not only on the parent cell somata but also on the proximal dendrites that extend into the other sublayer (Figure 1K). Therefore, the degree of preferential PVBC innervation of the deep sublayer (as seen with imaging) does not reflect the true degree of preferential PVBC innervation of individual dPCs (as assessed with paired recordings or bouton counts on individual PCs).

Functional Relevance and Outlook

The existence of nonuniform inhibitory and excitatory local microcircuits between PC subpopulations and PVBCs is likely to have profound consequences for the mechanisms by which local inhibition in CA1 regulates output from the hippocampus. In particular, our results demonstrating biased inhibitory and excitatory connections between PVBCs and differentially projecting dPCs may serve to facilitate the coordination of the hippocampus, MEC, mPFC, and AMG during mnemonic functions, where these brain regions interact during learning, consolidation, retrieval, and extinction. For example, the significantly larger PVBC innervation of $_{AMG}$dPCs versus $_{mPFC}$dPCs that we uncovered in the ventral hippocampus, together with the strikingly higher probability of local excitatory connections from $_{mPFC}$dPCs to PVBCs (Figure S5L), appear to be well-suited to provide a form of built-in, "automatic," preferential inhibition of the $_{AMG}$dPCs whenever the dPCs projecting from the hippocampus to the mPFC increase their activity. It is interesting to speculate that such local circuit arrangements may contribute to the extinction phase of the contextual gating of fear responses (e.g., Maren and Quirk, 2004), where recent results showed an increased output from the ventral hippocampus to the mPFC simultaneously with a depression in the ventral hippocampal excitatory drive to the AMG fear circuit (Sotres-Bayon et al., 2012; see Figure S5M). Selective optogenetic or DREADD-based manipulation of the ventral hippocampal circuits in fear-conditioned animals will need to be performed to carefully dissect the relative roles of the heterogeneous, biased excitatory-inhibitory circuitry involving the PVBCs and the differentially projecting dPCs in this process.

Our study also emphasizes the importance of future investigations into the detailed mechanisms by which these specialized local inhibitory-excitatory circuits are formed. Because neurogenesis of dPCs occurs earlier than sPCs (Baimbridge et al., 1991), and the development of parallel hippocampal excitatory channels involves PCs with distinct birthdates, synaptogenesis, and gene expression profiles (Deguchi et al., 2011), our results suggest that developmental mechanisms drive the formation of specialized microcircuits between the PC subpopulations and local circuit interneurons. Therefore, the sparse ensemble activity of the CA1 hippocampal output circuit may not be random but rather might reflect the parsing of the CA1 PC subpopulation by synaptic and intrinsic sources into heterogeneous groups that may contribute differentially to hippocampal memory functions.

EXPERIMENTAL PROCEDURES

All experiments were conducted in accordance with the Institutional Animal Care and Use Committee of the University of California, Irvine and Columbia University.

Mice

To target PV^+ interneurons for patch-clamp recordings, we crossed a PV-Cre line (The Jackson Laboratory stock 008069) with a reporter line (The Jackson Laboratory stock 007905) to produce mice expressing the red fluorescent protein tdTomato in PV^+ cells (PV-TOM mice). For optogenetic experiments, selective expression of excitatory channelrhodopsin (ChR2) in PV^+ interneurons was achieved by crossing PV-Cre line with mice expressing ChR2 Cre-dependently (The Jackson Laboratory stock 012569) (PV-ChR2 mice); in a subset of experiments, C57BL/6J mice were used. For additional information, see Supplemental Experimental Procedures.

Paired Recordings from In Vitro Slices

Coronal hippocampal slices (300 μm) were prepared from 2- to 3-month-old PV-TOM mice and C57BL/6J mice of either sex. Slices were incubated in sucrose-containing artificial CSF (ACSF) for an hour. After the initial incubation period, slices were transferred in the same ACSF solution used for recordings. All interneurons were identified post hoc as PVBCs or CCKBCs (see Supplemental Experimental Procedures: 3. Cell type identification). For paired recordings, whole-cell recordings in current clamp were obtained from PVBCs or CCKBCs (holding potential: −60 mV) with patch pipettes (3–5 MΩ) filled with internal solution containing 4 mM [Cl^-]. PCs (voltage clamp; holding potential: −70 mV) were recorded with internal solution containing 48.7 mM chloride (calculated $E_{GABA(A)}$ = −26.3 mV), except for Figures 4A and 4B (current clamp; pipettes contained 4 mM chloride; calculated $E_{GABA(A)}$ = −75.7 mV). In almost all pairs, we tested the PC-to-interneuron connections as well (PC, in the current-clamp configuration, holding potential −70 mV; interneurons, in voltage-clamp configuration, −70 mV). For additional information, see Supplemental Experimental Procedures.

In Vivo Calcium Imaging

PV-TOM mice were injected with serotype 1 (*rep/cap*: 2/1) rAAV [rAAV (*Synapsin-GCaMP5*)^{cre}] into the dorsal CA1. Mice 2 weeks postinjection were implanted with a chronic hippocampal imaging window above the left dorsal CA1 (Kaifosh et al., 2013). GCaMP5 fluorescence was imaged using a Ti:Sapphire laser tuned to 920 nm (Coherent) and a two-photon laser-scanning microscope (Prairie), focused at hippocampal tissue with a 40× objective (0.8 NA, Nikon). We collected imaging data using PrairieView software (Prairie) in concert with custom-designed hardware and software for behavioral readout and synchronization with imaging data. We imaged boutons at 256 × 128 pixels, 1.6 μs dwell time for 2,000–2,400 frames, a sufficient time to record several running bouts interspersed with periods of quiet. We used 165 × 165 μm FOVs for analysis of full-field ROIs (7.63 Hz; Figures 2B and 2C) and 82 × 82 μm or 41 × 41 μm FOVs for analysis of bouton ROIs (9.7 Hz and 10.2 Hz, respectively; Figures 2D and 2E). For in vivo anatomical measurements of bouton density, we anesthetized mice with ketamine/xylazine and imaged superficial and deep locations in 3–6 μm z stacks (82 × 82 μm FOV, 512 × 512 pixels, 6 μs dwell, 100 frames; Figure 2F). For additional information, see Supplemental Experimental Procedures.

Computational Model

We simulated a microcircuit containing 1,000 sPCs, 1,000 dPCs, and 36 PVBCs (a realistic ratio of neurons based on Bezaire and Soltesz, 2013) in NEURON (Carnevale and Hines, 2006). The models of each cell type, and the PC-PVBC and PVBC-PC connections, were constrained using anatomical and electrophysiological data. We injected PCs with tonic current to equalize their resting membrane potentials and then gave equal frequency and strength synaptic excitation to their strata Rad/Ori dendrites in the form of random, independent, Poisson-distributed inputs. PVBCs received synaptic inputs of the same nature as the PCs. Different excitation levels were achieved by increasing the number of Poisson inputs by the stated percentage to either the dPCs or sPCs. We ran three statistically independent versions of each simulation. The average firing rate of each cell type was first normalized to its control condition; then we compared normalized rates for each type. Model code is available at http://www.ivansolteszlab.org/models/superdeep.html. For details, see Supplemental Experimental Procedures.

Model Accessibility

The ModelDB accession number for the model code reported in this paper is 153280, available at http://senselab.med.yale.edu/ModelDB/ShowModel.asp?model=153280. We have also uploaded the latest development version of the code that is compatible with NeuroConstruct, along with NeuroML definitions for use in implementing the code in an alternate simulator such as GENESIS, to the Open Source Brain website, http://www.opensourcebrain.org/projects/nc_superdeep. In addition, the reader can download all the raw results data from our simulations, learn about our data analyses procedures, and examine the model components via an interactive graphic on our lab website at http://www.ivansolteszlab.org/models/superdeep.html.

Statistical Analysis

Paired or unpaired (as appropriate) two-tailed Student's t tests were used. In cases in which data did not show a normal distribution (i.e., failed the Shapiro-Wilk test), Wilcoxon's signed-rank or Mann-Whitney tests for paired and unpaired data, respectively, were used. Pearson's chi-square tests were used for the connection probability without (for two groups; Figures 1F, 3C, 3E, 3F, and 5D) or with Bonferroni-Holm multiple corrections (for three groups; Figure 6G). ANOVAs were followed by Tukey-Kramer tests for mean comparisons (Figures 6E and S5D). Tukey-Kramer tests were used for Figures 4D–4F. Data are presented as mean ± SEM. A p value < 0.05 was considered significant.

ACCESSION NUMBERS

The ModelDB accession number for the model code reported in this paper is 153280.

SUPPLEMENTAL INFORMATION

Supplemental Information includes Supplemental Experimental Procedures, five figures, and one table and can be found with this article online at http://dx.doi.org/10.1016/j.neuron.2014.03.034.

AUTHOR CONTRIBUTIONS

S.-H.L., I.M., A.L., and I.S. designed the experiments; S.-H.L. and I.M. performed the electrophysiological and morphological experiments and analysis; C.V. performed triple immunocytochemistry and in vivo filling of basket cells; M.B. carried out computational modeling; N.D., M.L.-B., and A.L. designed and performed the in vivo imaging experiments; S.-H.L., I.M., N.D., M.B., A.L., and I.S. wrote the paper.

ACKNOWLEDGMENTS

We thank R. Zhu, J. Varga, O. Rodriguez, M.K. Oberoi, A. Sharma, P. Kaifosh, A. Castro, and J. Zaremba for technical support, D.C. Lyon for assistance with Neurolucida System, and E. Krook-Magnuson, H. Kim, M. Maroso, Y.J. Kang, and C. Krook-Magnuson for generous advice. This work was supported by the U.S. National Institutes of Health (NS74432 to I.S.), National Science Foundation (DGE-0808392 to M.B.), University of California Irvine Center for Autism Research and Treatment (to I.S.), by Searle, Human Frontiers Science Program, McKnight Memory and Cognitive Disorders Award, and Harvey L. Karp Discovery Award (to A.L.), and NSERC postgraduate scholarship (to M.L.-B.). Computer modeling was supported by NSF's XSEDE program through the Neuroscience Gateway Portal for computational neuroscientists and via XSEDE Startup Allocations (TG-IBN100011 to M.B. and TG-IBN130022 to I.S.). Technical support and parallel computing time were

provided by the San Diego Supercomputing Center's Trestles computer, the University of Texas' Stampede computer, and the University of California Irvine's High Performance Computer.

Accepted: March 31, 2014
Published: May 15, 2014

REFERENCES

Akerboom, J., Chen, T.W., Wardill, T.J., Tian, L., Marvin, J.S., Mutlu, S., Calderón, N.C., Esposti, F., Borghuis, B.G., Sun, X.R., et al. (2012). Optimization of a GCaMP calcium indicator for neural activity imaging. J. Neurosci. *32*, 13819–13840.

Armstrong, C., and Soltesz, I. (2012). Basket cell dichotomy in microcircuit function. J. Physiol. *590*, 683–694.

Baimbridge, K.G., and Miller, J.J. (1982). Immunohistochemical localization of calcium-binding protein in the cerebellum, hippocampal formation and olfactory bulb of the rat. Brain Res. *245*, 223–229.

Baimbridge, K.G., Peet, M.J., McLennan, H., and Church, J. (1991). Bursting response to current-evoked depolarization in rat CA1 pyramidal neurons is correlated with lucifer yellow dye coupling but not with the presence of calbindin-D28k. Synapse *7*, 269–277.

Bannister, N.J., and Larkman, A.U. (1995). Dendritic morphology of CA1 pyramidal neurones from the rat hippocampus: I. Branching patterns. J. Comp. Neurol. *360*, 150–160.

Bezaire, M.J., and Soltesz, I. (2013). Quantitative assessment of CA1 local circuits: knowledge base for interneuron-pyramidal cell connectivity. Hippocampus *23*, 751–785.

Bodor, A.L., Katona, I., Nyíri, G., Mackie, K., Ledent, C., Hájos, N., and Freund, T.F. (2005). Endocannabinoid signaling in rat somatosensory cortex: laminar differences and involvement of specific interneuron types. J. Neurosci. *25*, 6845–6856.

Buzsáki, G., and Wang, X.J. (2012). Mechanisms of gamma oscillations. Annu. Rev. Neurosci. *35*, 203–225.

Carnevale, N.T., and Hines, M.L. (2006). The Neuron Book. (Cambridge: Cambridge University Press).

Cenquizca, L.A., and Swanson, L.W. (2007). Spatial organization of direct hippocampal field CA1 axonal projections to the rest of the cerebral cortex. Brain Res. Brain Res. Rev. *56*, 1–26.

Deguchi, Y., Donato, F., Galimberti, I., Cabuy, E., and Caroni, P. (2011). Temporally matched subpopulations of selectively interconnected principal neurons in the hippocampus. Nat. Neurosci. *14*, 495–504.

Fanselow, M.S., and Poulos, A.M. (2005). The neuroscience of mammalian associative learning. Annu. Rev. Psychol. *56*, 207–234.

Fariñas, I., and DeFelipe, J. (1991). Patterns of synaptic input on corticocortical and corticothalamic cells in the cat visual cortex. II. The axon initial segment. J. Comp. Neurol. *304*, 70–77.

Fino, E., and Yuste, R. (2011). Dense inhibitory connectivity in neocortex. Neuron *69*, 1188–1203.

Gibson, J.R., Huber, K.M., and Südhof, T.C. (2009). Neuroligin-2 deletion selectively decreases inhibitory synaptic transmission originating from fast-spiking but not from somatostatin-positive interneurons. J. Neurosci. *29*, 13883–13897.

Gittis, A.H., Nelson, A.B., Thwin, M.T., Palop, J.J., and Kreitzer, A.C. (2010). Distinct roles of GABAergic interneurons in the regulation of striatal output pathways. J. Neurosci. *30*, 2223–2234.

Graves, A.R., Moore, S.J., Bloss, E.B., Mensh, B.D., Kath, W.L., and Spruston, N. (2012). Hippocampal pyramidal neurons comprise two distinct cell types that are countermodulated by metabotropic receptors. Neuron *76*, 776–789.

Halasy, K., Buhl, E.H., Lörinczi, Z., Tamás, G., and Somogyi, P. (1996). Synaptic target selectivity and input of GABAergic basket and bistratified interneurons in the CA1 area of the rat hippocampus. Hippocampus *6*, 306–329.

Jarsky, T., Mady, R., Kennedy, B., and Spruston, N. (2008). Distribution of bursting neurons in the CA1 region and the subiculum of the rat hippocampus. J. Comp. Neurol. *506*, 535–547.

Jung, M.W., Wiener, S.I., and McNaughton, B.L. (1994). Comparison of spatial firing characteristics of units in dorsal and ventral hippocampus of the rat. J. Neurosci. *14*, 7347–7356.

Kaifosh, P., Lovett-Barron, M., Turi, G.F., Reardon, T.R., and Losonczy, A. (2013). Septo-hippocampal GABAergic signaling across multiple modalities in awake mice. Nat. Neurosci. *16*, 1182–1184.

Krook-Magnuson, E., Varga, C., Lee, S.H., and Soltesz, I. (2012). New dimensions of interneuronal specialization unmasked by principal cell heterogeneity. Trends Neurosci. *35*, 175–184.

Kuhlman, S.J., Olivas, N.D., Tring, E., Ikrar, T., Xu, X., and Trachtenberg, J.T. (2013). A disinhibitory microcircuit initiates critical-period plasticity in the visual cortex. Nature *501*, 543–546.

Lapray, D., Lasztoczi, B., Lagler, M., Viney, T.J., Katona, L., Valenti, O., Hartwich, K., Borhegyi, Z., Somogyi, P., and Klausberger, T. (2012). Behavior-dependent specialization of identified hippocampal interneurons. Nat. Neurosci. *15*, 1265–1271.

Lee, S.H., Földy, C., and Soltesz, I. (2010). Distinct endocannabinoid control of GABA release at perisomatic and dendritic synapses in the hippocampus. J. Neurosci. *30*, 7993–8000.

Lee, S.H., Kwan, A.C., Zhang, S., Phoumthipphavong, V., Flannery, J.G., Masmanidis, S.C., Taniguchi, H., Huang, Z.J., Zhang, F., Boyden, E.S., et al. (2012). Activation of specific interneurons improves V1 feature selectivity and visual perception. Nature *488*, 379–383.

Lee, A.T., Gee, S.M., Vogt, D., Patel, T., Rubenstein, J.L., and Sohal, V.S. (2014). Pyramidal neurons in prefrontal cortex receive subtype-specific forms of excitation and inhibition. Neuron *81*, 61–68.

Lewis, D.A., Hashimoto, T., and Volk, D.W. (2005). Cortical inhibitory neurons and schizophrenia. Nat. Rev. Neurosci. *6*, 312–324.

Maren, S., and Quirk, G.J. (2004). Neuronal signalling of fear memory. Nat. Rev. Neurosci. *5*, 844–852.

Mizuseki, K., Diba, K., Pastalkova, E., and Buzsáki, G. (2011). Hippocampal CA1 pyramidal cells form functionally distinct sublayers. Nat. Neurosci. *14*, 1174–1181.

Ogiwara, I., Miyamoto, H., Morita, N., Atapour, N., Mazaki, E., Inoue, I., Takeuchi, T., Itohara, S., Yanagawa, Y., Obata, K., et al. (2007). Nav1.1 localizes to axons of parvalbumin-positive inhibitory interneurons: a circuit basis for epileptic seizures in mice carrying an Scn1a gene mutation. J. Neurosci. *27*, 5903–5914.

Otsuka, T., and Kawaguchi, Y. (2009). Cortical inhibitory cell types differentially form intralaminar and interlaminar subnetworks with excitatory neurons. J. Neurosci. *29*, 10533–10540.

Packer, A.M., and Yuste, R. (2011). Dense, unspecific connectivity of neocortical parvalbumin-positive interneurons: a canonical microcircuit for inhibition? J. Neurosci. *31*, 13260–13271.

Pouille, F., and Scanziani, M. (2004). Routing of spike series by dynamic circuits in the hippocampus. Nature *429*, 717–723.

Slomianka, L., Amrein, I., Knuesel, I., Sørensen, J.C., and Wolfer, D.P. (2011). Hippocampal pyramidal cells: the reemergence of cortical lamination. Brain Struct. Funct. *216*, 301–317.

Soltesz, I. (2005). Diversity in the Neuronal Machine. (New York: Oxford University Press).

Sotres-Bayon, F., Sierra-Mercado, D., Pardilla-Delgado, E., and Quirk, G.J. (2012). Gating of fear in prelimbic cortex by hippocampal and amygdala inputs. Neuron *76*, 804–812.

Szabadics, J., Varga, C., Molnár, G., Oláh, S., Barzó, P., and Tamás, G. (2006). Excitatory effect of GABAergic axo-axonic cells in cortical microcircuits. Science *311*, 233–235.

Trouche, S., Sasaki, J.M., Tu, T., and Reijmers, L.G. (2013). Fear extinction causes target-specific remodeling of perisomatic inhibitory synapses. Neuron *80*, 1054–1065.

Varga, C., Lee, S.Y., and Soltesz, I. (2010). Target-selective GABAergic control of entorhinal cortex output. Nat. Neurosci. *13*, 822–824.

Varga, C., Golshani, P., and Soltesz, I. (2012). Frequency-invariant temporal ordering of interneuronal discharges during hippocampal oscillations in awake mice. Proc. Natl. Acad. Sci. USA *109*, E2726–E2734.

Verret, L., Mann, E.O., Hang, G.B., Barth, A.M., Cobos, I., Ho, K., Devidze, N., Masliah, E., Kreitzer, A.C., Mody, I., et al. (2012). Inhibitory interneuron deficit links altered network activity and cognitive dysfunction in Alzheimer model. Cell *149*, 708–721.

Viviani, D., Charlet, A., van den Burg, E., Robinet, C., Hurni, N., Abatis, M., Magara, F., and Stoop, R. (2011). Oxytocin selectively gates fear responses through distinct outputs from the central amygdala. Science *333*, 104–107.

Yoshimura, Y., and Callaway, E.M. (2005). Fine-scale specificity of cortical networks depends on inhibitory cell type and connectivity. Nat. Neurosci. *8*, 1552–1559.